Available online at www.sciencedirect.com
ScienceDirect
Journal of Power Sources 165 (2007) 9–15
JOURNAL OF POWER SOURCES
www.elsevier.com/locate/jpowsour

Electrochemical impedance studies on carbon supported PtRuNi and PtRu anode catalysts in acid medium for direct methanol fuel cell

Zhen-Bo Wang [a,*], Ge-Ping Yin [a], Yu-Yan Shao [a], Bo-Qian Yang [b], Peng-Fei Shi [a], Peter-Xian Feng [b]

[a] *Department of Applied Chemistry, Harbin Institute of Technology, Harbin 150001, China*
[b] *Department of Physics, University of Puerto Rico, P.O. Box 23343, San Juan, PR 00931, USA*

Received 26 October 2006; received in revised form 13 December 2006; accepted 13 December 2006
Available online 27 December 2006

Abstract

The anodic Pt–Ru–Ni/C and the Pt–Ru/C catalysts for potential application in direct methanol fuel cell (DMFC) were prepared by chemical reduction method. Electrochemical impedance spectroscopy (EIS) and cyclic voltammetry (CV) measurements were carried out by using a glassy carbon working electrode covered with the catalyst powder in a solution of 0.5 mol L^{-1} CH_3OH and 0.5 mol L^{-1} H_2SO_4 at 25 °C. EIS information discloses that the methanol electrooxidation on the Pt–Ru–Ni/C catalyst at various potentials shows different impedance behaviors. The mechanism and the rate-determining step of methanol electrooxidation are changed with increasing potential. Its rate-determining steps are the methanol dehydrogenation and the oxidation reaction of adsorbed intermediate CO_{ads} and OH_{ads} in low (400–500 mV) and high (600–800 mV) potentials, respectively. The catalytic activity of the Pt–Ru–Ni/C catalyst is higher for methanol electrooxidation than that of the Pt–Ru/C catalyst. Its tolerance performance to CO formed as one of the intermediates of methanol dehydrogenation is also better than that of the Pt–Ru/C catalyst.
© 2006 Elsevier B.V. All rights reserved.

Keywords: Direct methanol fuel cell; Electrochemical impedance; Pt–Ru–Ni/C catalyst; Pt–Ru/C catalyst; Methanol electrooxidation

1. Introduction

In the past decades, much attention has been paid to fuel cells because they offer a highly efficient and environmentally friendly technology for energy conversion. In particular, the development of low operating temperature polymer electrolyte proton exchange membrane fuel cell (PEMFC) for transportation applications has attracted attention [1]. The highest performance of PMFEC, where platinum is used as anode and cathode catalysts, is achieved with pure hydrogen and pure oxygen which are the preferred fuel for low temperature fuel cells. Although pure H_2 is an ideal fuel for PEMFC system, the storage systems for liquid or compressed H_2 are heavy, bulky and dangerous. Another obstacle is the lack of an infrastructure to distribute H_2 to the consumer [2,3]. These disadvantages have motivated fuel cell developers to look for alternatives. An alternative to the use of H_2 as fuel is small molecule hydrocarbons (such as methanol and ethanol), which are liquid fuel easy to handle and be used directly without prior reforming [4]. The direct methanol fuel cell (DMFC) can directly use aqueous methanol to be transformed to electrical current. Its structure system design is simple. However, presently achieved performance data of DMFC is not satisfying and material costs are too high. So, there is a need to improve the activity of catalysts for methanol electrooxidation and low the cost of DMFC [1,5,6].

The preparation of an efficient catalyst with high activity for methanol electrooxidation is related to the understanding of reactive mechanisms on its surface. The conventional electrochemical methods including polarization measurement, cyclic voltammetry (CV), Chronoamperometry, and stripping voltammetry are only employed to characterize the performance of the different catalysts [7–10]. It is difficult to use them to study an intrinsic reactive mechanism of methanol electrooxidation in the catalysts. However, the electrochemical impedance spectroscopy (EIS) technique is a good tool to analyze the kinetics of electrode reactions. This is the major advantage of this method

* Corresponding author. Present address: Department of Chemistry, University of Puerto Rico, Rio Piedras Campus, San Juan, PR 00931, USA.
Tel.: +1 787 764 0000X7465; fax: +1 787 764 1588.
E-mail address: wangzhenbo1008@yahoo.com.cn (Z.-B. Wang).

0378-7753/$ – see front matter © 2006 Elsevier B.V. All rights reserved.
doi:10.1016/j.jpowsour.2006.12.027

for the data interpretation as every parameter in the impedance expression has a clear physical significance related to the reaction mechanism. Therefore, the EIS technique has been used to investigate reaction mechanism [11–14], CO-tolerance for different Pt-based alloy catalysts [1,2], Nafion loading in the catalyst layer [15], and characteristics of membrane electrode assembly (MEA) [16,17].

At present, novel methods for preparing new alloy catalysts are investigated. In our previous publications, the novel carbon supported Pt–Ru–Ni catalyst was reported for methanol and ethanol electrooxidation [6,18,19]. The research with conventional electrochemical methods showed the catalytic activity of the Pt–Ru–Ni/C catalyst for methanol and ethanol electrooxidation was higher than that of the Pt–Ru/C catalyst. The new homemade Pt–Ru–Ni/C catalyst was characterized by EIS technique combined with CV in this paper. The aim of this work is to use EIS as a dynamic method for the mechanism discrimination of methanol electrooxidation and a comparison of the performance of the different catalysts.

2. Experimental

2.1. Preparation of catalysts

The Pt–Ru–Ni/C catalyst was prepared according to the method mentioned in the literatures [6,18,19]. As described briefly, the carbon black powder (Vulcan XC-72, Cabot) was used as a support for the catalysts. The samples contained 20% metals in weight of the catalysts were dispersed in the powder. The Pt–Ru (with an atomic ratio of 1:1)/C or the Pt–Ru–Ni (with an atomic ratio of 6:3:1)/C catalyst [18], 0.25 g, was obtained by chemical reduction with sodium borohydride of H_2PtCl_6, $RuCl_3$, and $NiCl_2$ as precursors at 80 °C. The carbon black was ultrasonically dispersed in a mixture of ultrapure water and isopropyl alcohol for 20 min. The precursors were added to the ink and then mixed thoroughly for 15 min. The pH value of the ink was adjusted to 8 by NaOH solution and then raised its temperature to 80 °C. Fifteen microlitres of 0.2 mol L^{-1} solution of sodium borohydride was added into the ink drop by drop and the bath was stirred for 1 h. The mixture was cooled, dried and washed repeatedly with ultrapure water (18.2 MΩ cm) until no Cl^- ions existed. The catalyst powder was dried for 3 h at 120 °C and stored in a vacuum vessel. All chemicals used were of analytical grade.

2.2. Preparation of working electrode and its electrochemical measurements

2.2.1. Preparation of working electrode

Glassy carbon working electrodes, 3 mm in diameter (electrode area 0.0706 cm^2), polished with 0.05 μm alumina to a mirror-finish before each experiment, were used as substrates for the carbon supported catalysts. For the electrode preparation, 5 μL of an ultrasonically redispersed catalyst suspension was pipetted onto the glassy carbon substrate. After the solvent evaporation, the deposited catalyst (28 $\mu g_{metal}\ cm^{-2}$) was covered with 5 μL of a dilute aqueous Nafion solution (5 wt.%). The resulting Nafion film with a thickness of ≤0.2 μm had a sufficient strength to attach the carbon particles permanently to the glassy carbon electrode without producing film diffusion resistances [20,21]. The Faradaic impedance of the film electrode was measured without mass transport limitations in order to investigate the kinetics and the mechanism of methanol electrooxidation.

2.2.2. Electrochemical measurements

Electrochemical measurements were carried out with a conventional three-electrode electrochemical cell at 25 °C. The glassy carbon thin film electrode as the working electrode (electrode area 0.0706 cm^2) was covered with the catalyst powder. A piece of Pt foil of 1 cm^2 area was used as the counter one. The reversible hydrogen electrode (RHE) was used as the reference one with its solution connected to the working electrode by a Luggin capillary whose tip was placed appropriately close to the working electrode. All potential values are versus RHE. All chemicals used were of analytical grade. All the solutions were prepared with ultrapure water (MilliQ, Millipore, 18.2 MΩ cm). A solution of 0.5 mol L^{-1} CH_3OH and 0.5 mol L^{-1} H_2SO_4 was stirred constantly and purged with ultrapure argon gas. Electrochemical experiments were performed using a CHI604B electrochemical analysis instrument. Cyclic voltammogram (CV) was plotted within a potential range from 0.05 to 1.2 V with a scanning rate of 1 mV s^{-1}. EIS were usually obtained at frequencies between 100 kHz and 0.01 Hz with 12 points per decade. The amplitude of the sinusoidal potential signal was 5 mV. Due to a slight contamination from the Nafion film, the working electrodes were electrochemically cleaned by continuous cycling at 50 mV s^{-1} until a stable response was obtained before the measurement curves were recorded.

3. Results and discussion

3.1. Impedance patterns on the Pt–Ru–Ni/C catalyst

In this section, the EIS technique was used to investigate the catalytic activity for the methanol electrooxidation on the anodic Pt–Ru–Ni/C catalyst surface. The EIS (A) and the phase shift (B) of methanol electrooxidation on the Pt–Ru–Ni/C catalyst at different potentials are shown in Figs. 1–3, respectively. The EIS results indicate that the methanol electrooxidation on the Pt–Ru–Ni/C catalyst at various potentials shows different impedance behaviors. The very similar impedance trends were observed on the Pt/C thin film electrode for methanol electrooxidation [22], Pt–Sn anode [2], and polymer electrolyte membrane fuel cells for H_2/CO electrooxidation [1,13,23,24]. A large arc shown in Fig. 1A reveals a slow reaction rate of methanol dehydrogenation oxidation [22]. It is understood that the slow kinetics is caused by the intermediate CO_{ads} from methanol dehydrogenation which are strongly adsorbed on Pt sites and block continuous adsorption and dehydrogenation of methanol molecules [22,25]. With increasing potential, the diameter of arc decreases rapidly, indicating that the charge transfer resistance for the methanol electrooxidation becomes smaller. Only

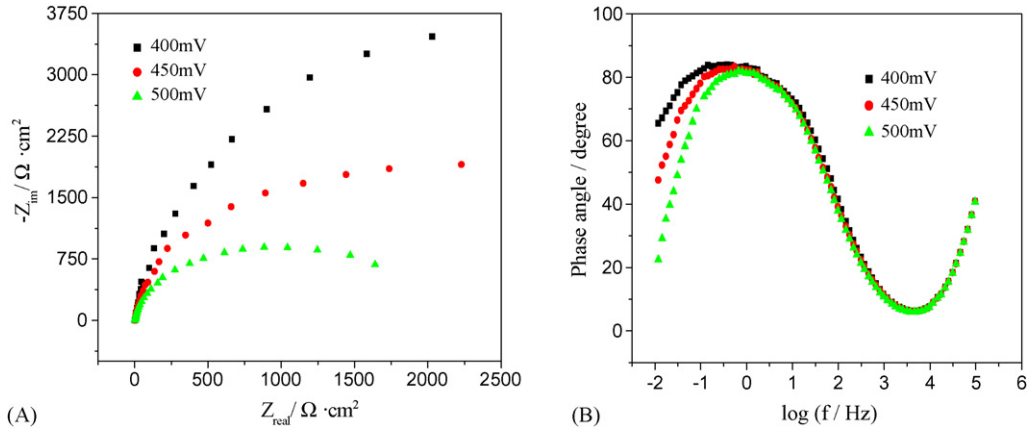

Fig. 1. Impedance patterns (A) and phase shift plots (B) of methanol electrooxidation in an Ar-saturated solution of 0.5 mol L^{-1} CH_3OH and 0.5 mol L^{-1} H_2SO_4 at 25 °C on the Pt–Ru–Ni/C catalyst at low potentials range (400–500 mV).

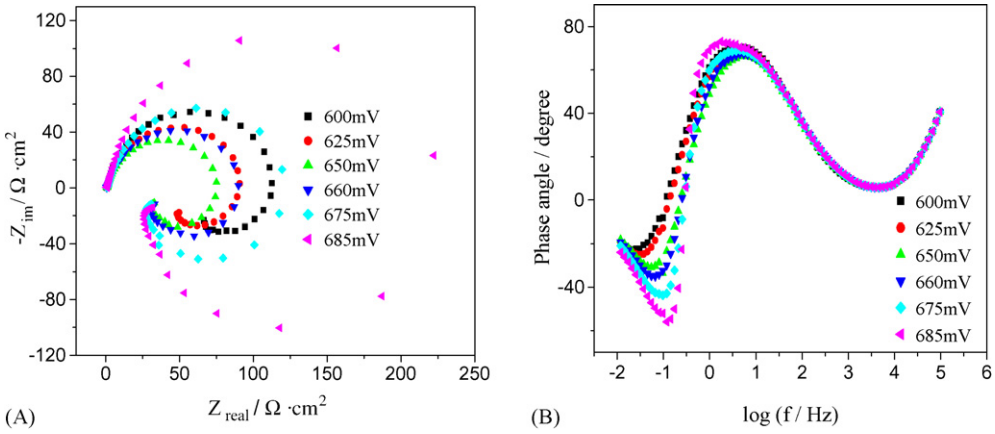

Fig. 2. Impedance patterns (A) and phase shift plots (B) of methanol electrooxidation in an Ar-saturated solution of 0.5 mol L^{-1} CH_3OH and 0.5 mol L^{-1} H_2SO_4 at 25 °C on the Pt–Ru–Ni/C catalyst at medium potentials range (600–685 mV).

one broad peak can be observed at low potentials as shown in Fig. 1B, indicating that only one reaction happens on the electrode surface, i.e. methanol dehydrogenation reaction. With the increase of the potential, the phase angle decreases gradually, the peak shifts toward higher frequency regions. The changing order is the same as that of EIS spectra.

A so-called 'pseudo-inductive' behavior begins to emerge in the impedance plots, where a large positive loop at higher frequency is accompanied by a small loop in the 4th quadrant at low frequency, with both diameters of the loops decreasing rapidly with the increase of the potential between 600 and 650 mV as shown in Fig. 2A. An explanation for the occurrence

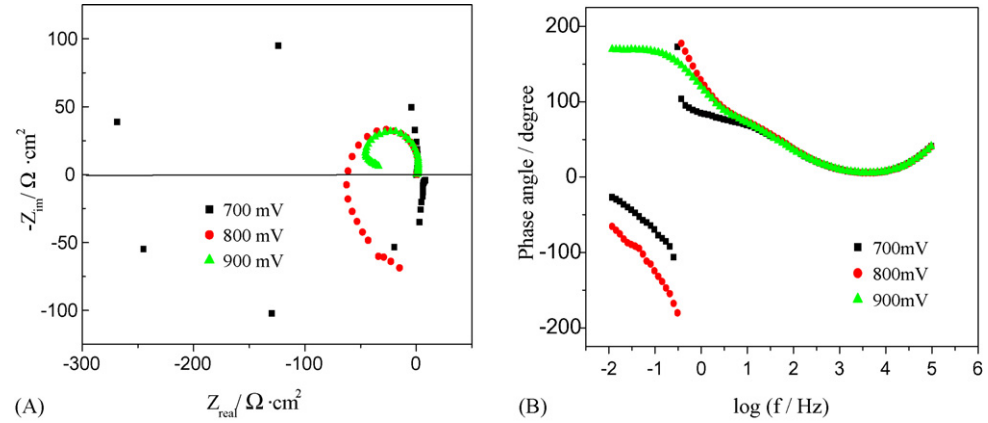

Fig. 3. Impedance patterns (A) and phase shift plots (B) of methanol electrooxidation in an Ar-saturated solution of 0.5 mol L^{-1} CH_3OH and 0.5 mol L^{-1} H_2SO_4 at 25 °C on the Pt–Ru–Ni/C catalyst at high potentials range (700–900 mV).

of inductive behavior during methanol electrooxidation can be elucidated [4,22]: the active sites on platinum are covered initially with the CO_{ads} layer formed as one of the intermediates of methanol dehydrogenation, and thus deactivated at lower potentials. As potential increases, some of the weakly CO_{ads} begin to be oxidized, producing Pt active sites in the adsorbed CO layer. Subsequent methanol molecules then can be adsorbed in these active sites. Consequently, the reaction rate of methanol electrooxidation is sharply increasing. Namely, the so-called 'pseudo-inductive' behavior results from the 'relaxation phenomenon' between adsorption–dehydrogenation of methanol molecules and oxidation–adsorption of the CO-like species.

The both diameters of the high and the low frequency arcs in the 1st and 4th quadrant increasing with the potential in the impedance plots are observed at potentials range, from 650 to 685 mV as shown in Fig. 2A. But the negative peak in phase shift plots begins to appear at 600 mV, namely appears both for the positive and negative maximum of the phase angle. With the increase of the potential, the shift of the negative peak is more rapid to a high frequency and becomes more and more acuminous, so that the two maximum peaks are closer at higher voltage as shown in Fig. 2B. It may be a result from the change of the rate-determining step of methanol electrooxidation.

As potentials arrive at 700–800 mV, a sudden change of impedance plots happens, with the two loops reversing to the 2nd and 3rd quadrants as shown in Fig. 3A. And with the increase of the potential, the diameters of both loops decrease. The two unattached positive and negative values of phase angle appear as shown in Fig. 3B. The main reason is that the rate-determining step changes from the methanol dehydrogenation to the oxidation removal of CO_{ads} by OH_{ads}, which leads to the reversal of impedance to the 2nd and 3th quadrants, i.e. the abrupt jumps of phase angle [22]. With continuous increasing potential, at 900 mV, the impedance plot only appears the 2nd quadrant. The phase angle at low frequency changes into a higher positive value.

A lot of work has been focused on the methanol electrooxidation with Pt-based catalysts [26–30]. It is well known that the addition of metal (denoted as Me) to Pt catalyst significantly lowers the overpotenital for methanol electrooxidation reaction through a so-called 'bifunctional mechanism' that can be summarized as follows [31–34]:

$$Pt + CH_3OH_{bulk} \rightarrow Pt\text{–}(CH_3OH)_{ads} \quad (1)$$

$$Pt\text{–}(CH_3OH)_{ads} \rightarrow Pt\text{–}CO_{ads} + 4H^+ + 4e^- \quad (2)$$

$$Me + H_2O \rightarrow Me\text{–}(H_2O)_{ads} \quad (3)$$

$$Me\text{–}(H_2O)_{ads} \rightarrow Me\text{–}(OH)_{ads} + H^+ + e^- \quad (4)$$

$$Pt\text{–}CO_{ads} + Me\text{–}(OH)_{ads} \rightarrow CO_2 + Pt + Me + H^+ + e^- \quad (5)$$

When Me–OH is generated by dissociative adsorption of H_2O on the catalyst surface, methanol oxidation proceeds as shown by arrow A in Fig. 4. However, strong adsorption of OH on the Pt surface at higher potentials inhibits further methanol electrooxidation, thus methanol electrooxidation peaks are observed

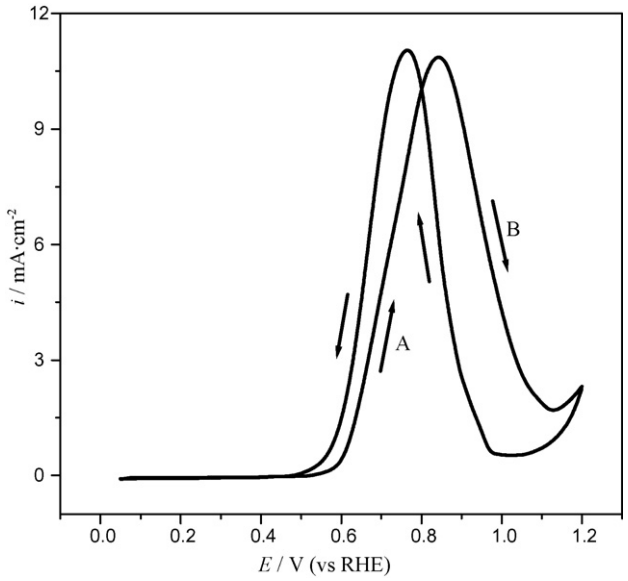

Fig. 4. The cyclic voltammetry curve of methanol electrooxidation on the Pt–Ru–Ni/C catalyst with a solution of 0.5 mol L^{-1} CH_3OH and 0.5 mol L^{-1} H_2SO_4 at 25 °C. Scan rate: 1 mV s^{-1}.

during positive potential scanning. When the potential scanning is reversed, the strongly adsorbed OH is reduced with potential lowering. Then methanol electrooxidation occurs again, thus its oxidation peak is observed at negative potential scanning as shown in Fig. 4. It can be seen from Fig. 4 that the onset potential of a current rise for methanol electrooxidation on the Pt–Ru–Ni/C catalyst is about 600 mV, which is similar to EIS measurement that reveals the CO_{ads} evidently oxidized at almost the same potential as shown in Fig. 2. Thus, the appearance of a 'pseudo-inductive' in EIS patterns is a proof that the CO coverage starts rapidly decreasing at this potential [24]. The peak potential for methanol electrooxidation, at which the peak current occurs is 842 mV (versus RHE), and the peak current density is 10.9 mA cm^{-2} during positive potential scanning on the Pt–Ru–Ni/C catalyst. The peak potential and the peak current density on the catalyst are about 765 mV (versus RHE) and 11.0 mA cm^{-2}, respectively, during its reverse scanning.

Comparison of the impedance plots, CV curve, and 'bifunctional mechanism' of methanol electrooxidation, it indicates that the surface sites of catalyst are mostly occupied by the adsorbed CO formed as one of the intermediates of methanol electrooxidation and thus deactivated at low potentials (400–500 mV) [22,25,35]. The rate-determining step of methanol electrooxidation is the methanol dehydrogenation (reaction (2)). So, there are only capacitive behaviors from double layer charge in the impedance plots.

With the increase of the potential, the CO_{ads} from methanol dehydrogenation are oxidized gradually. The active sites on platinum, which the adsorbed CO is cleaned up, continue to absorb and oxidize methanol molecules. So, there are inductive behaviors in the impedance plots that emerge in the 1st and 4th quadrants. Namely, the so-called 'pseudo-inductive' behavior is caused by the 'relaxation phenomenon' the oxidation of CO_{ads} coupled with further adsorption–dehydrogenation of methanol

molecules on the surface sites freed up by the CO_{ads} as shown in Fig. 2A. The current density of methanol electrooxidation is increasing as shown by arrow A in Fig. 4. The rate-determining step of methanol electrooxidation is thought to be the CO_{ads} oxidation on Pt active sites at the potential range of 600–650 mV (reaction (5)). With the continuous increase of the potential, the number of OH_{ads} is gradually increasing not only at Ru and Ni sites, but also at Pt sites, the rate-determining step may be thought to be the OH_{ads} oxidation removal at the potential range of 660–685 mV (reaction (5)). But, the gross ratio of methanol electrooxidation is increasing as shown by arrow A in Fig. 4. Namely, it is a result that the species of rate-determining step of methanol electrooxidation changes from CO_{ads} oxidation to OH_{ads} oxidation removal. Generally, the two peaks represent the existence of two time constants in phase shift plot as shown in Fig. 2B. The high frequency time constant corresponds to fast reaction step in an electrode process and the low frequency time constant corresponds to slow reaction step [4]. For the current electrode processes, the high frequency and low frequency time constants can be related to the methanol dehydrogenation (reaction (2)) and the rate of the oxidation removal of CO_{ads} by OH_{ads} (reaction (5)), respectively [18]. The approaching of the two peaks with the potential increasing indicates that the rates of the two reaction processes are getting closer. As the potential reaches 700 mV, due to the surface sites of catalyst are covered by the OH_{ads}, the rates of the methanol molecules absorbed and oxidized gets slow and difficult. The change of the rate-determining step leads to the abrupt jump of phase angel and the reversal of impedance to the 2nd and 3th quadrants as shown in Fig. 3. As the potential reaches 900 mV, the surface sites of catalyst are covered with more OH_{ads}, the current density of methanol electrooxidation is getting small as shown by arrow B in Fig. 4. The oxygen evolution happens in the surface of the Pt–Ru–Ni/C catalyst. There is one time constant in the phase shift plot. The phase angle markedly increases.

3.2. Comparison of the performance on the Pt–Ru–Ni/C and the Pt–Ru/C catalysts

The impedance patterns on the Pt–Ru/C catalyst are similar to those on the Pt–Ru–Ni/C catalyst (they are not shown in this paper). These are opposite to the EIS of CO-tolerance for the Pt–Ru/C at the high potentials, which no EIS appeared in the 2nd and 3rd quadrants [2].

The impedance patterns on the Pt–Ru–Ni/C and the Pt–Ru/C catalysts in an Ar-saturated solution of 0.5 mol L^{-1} CH_3OH and 0.5 mol L^{-1} H_2SO_4 at 25 °C at 400, 650 and 800 mV are shown in Figs. 5–7, respectively. The Faradaic admittance (the inverse of the Faradaic impedance) of methanol electrooxidation is [25]:

$$Y_F = \frac{1}{R_{ct}} + \frac{B}{a + j\omega} \quad (6)$$

where $R_{ct} = (\partial E/\partial I_F)_{ss}$ is charge transfer resistance of the electrode reaction. Its value is always positive. The subscript "ss" stands for steady state. I_F denotes the Faraday current. It can be seen from Figs. 5–7 that the reaction resistances (R_{ct})

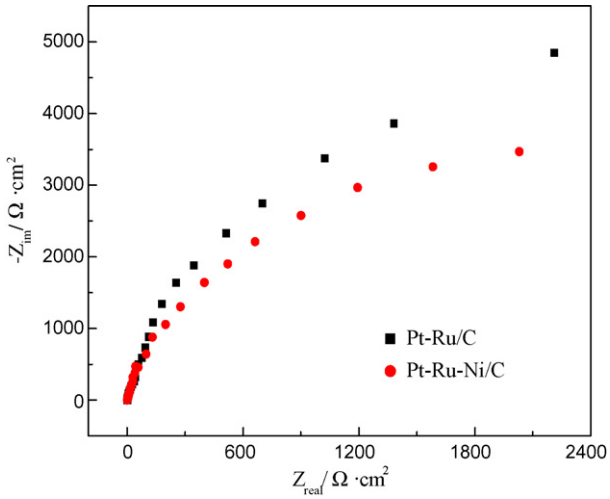

Fig. 5. Impedance patterns of methanol electrooxidation on the Pt–Ru–Ni/C and the Pt–Ru/C catalysts in an Ar-saturated solution of 0.5 mol L^{-1} CH_3OH and 0.5 mol L^{-1} H_2SO_4 at 25 °C at 400 mV.

for methanol electrooxidation on the Pt–Ru–Ni/C catalyst are smaller than those of the Pt–Ru/C catalyst.

It indicates in Fig. 5 that the rate of methanol dehydrogenation is faster on the Pt–Ru–Ni/C catalyst. Thus, the performance of CO-tolerance on the Pt–Ru–Ni/C catalyst is higher than that on the Pt–Ru/C catalyst. It reveals from Figs. 6 and 7 that the rates of oxidation removal of the CO_{ads} by OH_{ads} are rapid on the Pt–Ru–Ni/C catalyst, i.e. its catalytic activity for methanol electrooxidation are higher than that of the Pt–Ru/C catalyst. Those results are similar to those of the measurements with conventional electrochemical methods in our previous works [18,19].

The electron transfer from nickel to platinum in Pt–Ni is in agreement with the electronegativity series for Ni and Pt, i.e. 1.91 and 2.28, respectively. The electron transfer may contribute to the decay of the Pt–CO binding energy and improve

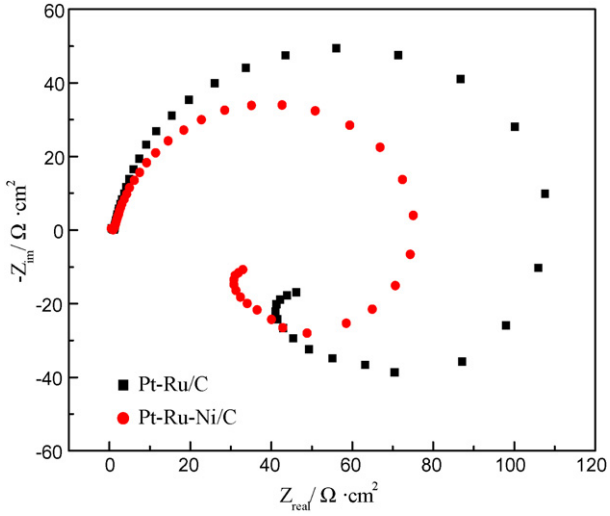

Fig. 6. Impedance patterns of methanol electrooxidation on the Pt–Ru–Ni/C and the Pt–Ru/C catalysts in an Ar-saturated solution of 0.5 mol L^{-1} CH_3OH and 0.5 mol L^{-1} H_2SO_4 at 25 °C at 650 mV.

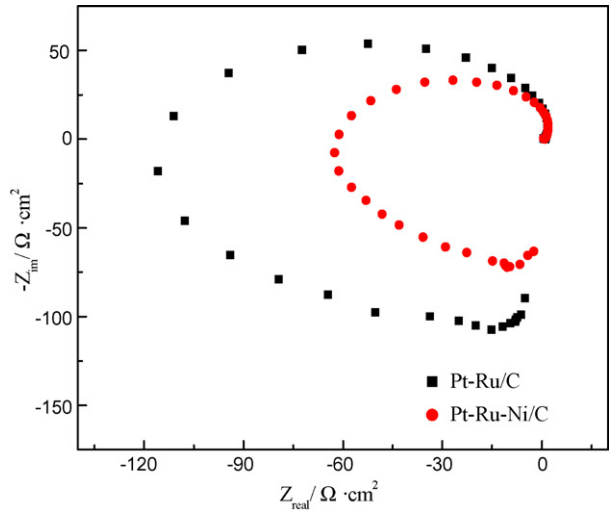

Fig. 7. Impedance patterns of methanol electrooxidation on the Pt–Ru–Ni/C and the Pt–Ru/C catalysts in an Ar-saturated solution of 0.5 mol L^{-1} CH_3OH and 0.5 mol L^{-1} H_2SO_4 at 25 °C at 800 mV.

oxidation of CO-like intermediates from methanol dehydrogenation, and enhance the adsorption and oxidation of methanol molecules [18,19,36]. Furthermore, the surface layer containing both $Ni(OH)_2$ and NiOOH is formed on the Pt–Ru–Ni metal particles [36,37]. The Ni hydroxide layer has favorable proton and electronic conductivities, and well protects the bulk from corrosion under methanol electrooxidation conditions [36,37]. Such a hydroxide layer on Pt–Ru–Ni alloy may display high catalytic activity with respect to methanol electrooxidation due to the formation of oxygen-containing (OH_{ads}) species on the catalyst, and such species transform CO-like poisoning species on Pt into CO_2, leaving the active sites on Pt for further adsorption and oxidation of methanol molecules. Lately, the research was presented that the hydrogen spillover from the Pt sites to the neighboring NiOOH on the surface of Pt–Ru–Ni/C nanocomposite played an important role in improving CO_{ads} electrooxidation for PEMFC [38]. The obtained results indicate that the addition of Ni into Pt–Ru catalysts can significantly improve the electrode performance for methanol electrooxidation. The research of an intrinsic mechanism in this catalyst is in progress.

4. Conclusions

Electrocatalytic activity of the Pt–Ru–Ni/C catalyst, formed by reduction with $NaBH_4$ of the inorganic salt precursors, was investigated by the EIS with respect to the methanol electrooxidation in H_2SO_4 solution. The impedance patterns for methanol electrooxidation reveal that three processes occur at the interface of the Pt–Ru–Ni/C catalyst: one is associated with the methanol dehydrogenation step at low potentials (400–500 mV); the second at medium potentials (600–800 mV) is assigned to oxidation of intermediate species, i.e. the oxidation removal of CO_{ads} by OH_{ads}; the third is considered as oxygen evolution at high potentials (900 mV). The experimental data reported in this paper indicate that the performance of the Pt–Ru–Ni/C catalyst for methanol electrooxidation is much better than that of the Pt–Ru/C catalyst due to promoting function of Ni. The results of EIS measurement, which the performance of two catalysts was compared, were consistent with those of the conventional electrochemical methods [19].

Acknowledgements

This work is supported financially by the National Natural Science Foundation of China (Grant No. 20606007), Heilongjiang Natural Science Foundation (B0201), and Harbin Institute of Technology (HIT.2002.39).

References

[1] N. Wagner, M. Schulze, Electrochim. Acta 48 (2003) 3899.
[2] Y.-J. Leng, X. Wang, I.-M. Hsing, J. Electroanal. Chem. 528 (2002) 145.
[3] S.J.C. Cleghorn, T.E. Springer, M.S. Wilson, C. Zawodzinski, T.A. Zawodzinski, S. Gottesfeld, Int. J. Hydrogen Energy 22 (1997) 1137.
[4] X. Wang, I.-M. Hsing, Y.-J. Leng, P.-L. Yue, Electrochim. Acta 46 (2001) 4397.
[5] Z.-B. Wang, G.-P. Yin, P.-F. Shi, Carbon 44 (2006) 133.
[6] Z.-B. Wang, G.-P. Yin, J. Zhang, Y.-C. Sun, P.-F. Shi, J. Power Sources 160 (2006) 37.
[7] Q.-Y. Lu, B. Yang, L. Zhuang, J.T. Lu, J. Phys. Chem. B 109 (2005) 1715.
[8] W.-Z. Li, X. Wang, Z.-W. Chen, M. Waje, Y.-S. Yan, J. Phys. Chem. B 110 (2006) 15353.
[9] S. Jayaraman, T.F. Jaramillo, S.-H. Baeck, E.W. McFarland, J. Phys. Chem. B 109 (2005) 22958.
[10] Y.-Y. Shao, G.-P. Yin, J.J. Wang, Y.Z. Gao, P.-F. Shi, J. Electrochem. Soc. 153 (2006) A1261.
[11] U. Krewer, M. Christov, T. Vidakovic, K. Sundmacher, J. Electroanal. Chem. 589 (2006) 148.
[12] D.A. Harrington, B.E. Conway, Eletrochim. Acta 32 (1987) 1703.
[13] J.-M. Hu, J.Q. Zhang, C.-N. Cao, I.-M. Hsing, Electrochim. Acta 49 (2004) 5227.
[14] R.E. Melnick, G.T.R. Palmore, J. Phys. Chem. B 105 (2001) 9449.
[15] E. Antolini, L. Giorgi, A. Pozio, E. Passalacqua, J. Power Sources 77 (1999) 136.
[16] Y.C. Liu, X.P. Qiu, W.T. Zhu, G.S. Wu, J. Power Sources 114 (2003) 10.
[17] J.M. Song, S.Y. Cha, W.M. Lee, J. Power Sources 94 (2001) 78.
[18] Z.-B. Wang, G.-P. Yin, P.-F. Shi, Y.-C. Sun, Electrochem. Solid State Lett. 9 (2006) A13.
[19] Z.-B. Wang, G.-P. Yin, J. Zhang, Y.-C. Sun, P.-F. Shi, Electrochim. Acta 51 (2006) 5691.
[20] T.J. Schmidt, H.A. Gasteiger, G.D. Stab, P.M. Urban, D.M. Kolb, R.J. Behm, J. Electrochem. Soc. 145 (1998) 2354.
[21] Z.-B. Wang, G.-P. Yin, P.-F. Shi, J. Electrochem. Soc. 152 (2005) A2406.
[22] I.-M. Hsing, X. Wang, Y.-J. Leng, J. Electrochem. Soc. 149 (2002) A615.
[23] N. Wagner, E. Gülzow, J. Power Sources 127 (2004) 341.
[24] M. Ciureanu, H. Wang, J. Electrochem. Soc. 146 (1999) 4031.
[25] G. Wu, L. Li, B.-Q. Xu, Electrochim. Acta 50 (2004) 1.
[26] L. Giorgi, A. Pozio, C. Bracchini, R. Giorgi, S. Turtu, J. Appl. Electrochem. 31 (2001) 325.
[27] A. Pozio, M. de Francesco, A. Cemmi, F. Cardellini, L. Giorgi, J. Power Sources 105 (2002) 13.
[28] C.L. Green, A. Kucernak, J. Phys. Chem. B 106 (2002) 1036.
[29] S.A. Kirillov, P.E. Tsiakaras, I.V. Romanova, J. Mol. Struct. 651–653 (2003) 365.
[30] A.V. Tripkovic, K.D. Popovic, J.D. Lovic, Electrochim. Acta 46 (2001) 3163.
[31] B. Beden, F. Kadirgan, C. Lamy, J.M. Leger, J. Electroanal. Chem. 127 (1989) 75.
[32] T. Page, R. Johnson, J. Hormes, S. Noding, B. Rambabu, J. Electroanal. Chem. 485 (2000) 341.

[33] A.T. Haug, R.E. White, J.W. Weidner, W. Huang, J. Electrochem. Soc. 149 (2002) A862.
[34] L.X. Yang, C. Bock, B. Macdougall, J. Park, J. Appl. Electrochem. 34 (2004) 427.
[35] L. Dubau, F. Hahn, C. Coutanceau, J.-M. Leger, C. Lamy, J. Electroanal. Chem. 554/555 (2003) 407.
[36] K.W. Park, J.H. Choi, B.K. Kwon, S.A. Lee, Y.E. Sung, H.Y. Ha, S.A. Hong, H.S. Kim, A. Wieckowski, J. Phys. Chem. B 106 (2002) 1869.
[37] K.W. Park, J.H. Choi, Y.E. Sung, J. Phys. Chem. B 107 (2003) 5851.
[38] Y.M. Liang, H.M. Zhang, Z.Q. Tian, X.B. Zhu, X.L. Wang, B.L. Yi, J. Phys. Chem. B 110 (2006) 7828.